Molecular BioSystems

RSC Publishing

PAPER

View Article Online
View Journal | View Issue

Redox-proteomic analysis of doxorubicin-induced altered thiol activity in cardiomyocytes†

Cite this: *Mol. BioSyst.*, 2013, **9**, 447

Szu-Ting Lin,[a] Hsiu-Chuan Chou,[b] Yi-Wen Chen[a] and Hong-Lin Chan*[a]

Received 12th September 2012,
Accepted 21st December 2012

DOI: 10.1039/c2mb25367d

www.rsc.org/molecularbiosystems

Doxorubicin is an anticancer drug used in a wide range of cancer therapies, yet some side effects have been reported. One of these is cardiotoxicity, including cardiomyopathy and ultimately congestive heart failure. This damage to the heart has been shown to result from doxorubicin-induced reactive oxygen species. However, the cellular targets of doxorubicin-induced oxidative damage on cardiomyocytes are largely unknown. For this, a cysteine-labeling-based two-dimensional difference gel electrophoresis (2D-DIGE) combined with MALDI-TOF/TOF mass spectrometry (MALDI-TOF/TOF MS) were employed to analyze the impact of doxorubicin treatment on the redox regulation in rat cardiomyocytes. This study demonstrated 25 unique protein features that had significantly changed in their thiol reactivity and revealed that doxorubicin-induced cardiotoxicity involves dysregulation of protein folding, translational regulation and cytoskeleton regulation. Our work shows that this combined proteomic strategy provides a rapid method to study the molecular mechanisms of doxorubicin-induced cytotoxicity in the heart. The identified targets may be useful for further evaluation as potential cardiotoxic biomarkers during damage to the heart induced by doxorubicin, as well as possible diagnostic or therapeutic applications.

1. Introduction

Doxorubicin is one of the anticancer drugs used in the treatment of a number of cancers, such as breast cancer, lung cancer and many other carcinoma types.[1–3] Doxorubicin's exact mechanism of action is complex; for example, it interacts with DNA by intercalation to inhibit the synthesis of DNA and RNA. Additionally, some side effects of doxorubicin have been reported, and one of these is cardiotoxicity, including cardiomyopathy and ultimately congestive heart failure.[4] Although the details of the causal mechanism of doxorubicin-induced cardiotoxicity remains largely unclear, most of the evidence shows that doxorubicin is reduced to its semiquinone form by the mitochondria electron transport system. The semiquinone subsequently reacts with oxygen, iron and hydrogen peroxide to produce reactive oxygen species leading to cell apoptosis and myocyte damage.[5,6]

Proteomics is a powerful tool to monitor protein expression and protein activity changes in response to a specific treatment. 2-DE remains an important technique in proteomics for global protein profiling within biological samples and plays a complementary role to LC-MS-based analysis. However, reliable quantitative comparison between gels remains the primary challenge in 2-DE analysis. A significant improvement in gel-based protein detection and quantification was achieved by the introduction of 2D-DIGE, where several samples can be co-detected on the same gel using differential fluorescent labeling. This approach alleviates gel-to-gel variation and allows comparison of the relative amount of resolved proteins across different gels using a fluorescently-labeled internal standard. Moreover, the 2D-DIGE technique has the advantages of a broader dynamic range of detection, higher sensitivity and greater reproducibility than traditional 2-DE.[7] Recently, a cysteine-labeling version of 2D-DIGE was developed using ICy dyes (iodoacetyl cyanine dyes), which react with the free thiol group of cysteines *via* alkylation. A pair of ICy dyes (ICy3 and ICy5) have been used to monitor redox-dependent protein thiol modifications in model cell systems.[8–10]

The aim of this investigation was to conduct an *in vitro* investigation into doxorubicin-induced cardiotoxicity using quantitative redox-proteomic strategies, including ICy dyes-based labeling and MALDI-TOF MS, to monitor redox-dependent protein thiol modifications, to increase our understanding of the molecular processes involved, and to identify potential cardiotoxic biomarkers with possible diagnostic or therapeutic applications.

[a] *Department of Medical Science and Institute of Bioinformatics and Structural Biology, National Tsing Hua University, No. 101, Kuang-Fu Road. Sec. 2, Hsinchu 30013, Taiwan. E-mail: hlchan@life.nthu.edu.tw; Fax: +886-3-5715934; Tel: 886-3-5742476*
[b] *Department of Applied Science, National Hsinchu University of Education, Hsinchu, Taiwan*

† Electronic supplementary information (ESI) available. See DOI: 10.1039/c2mb25367d

2. Materials and methods

2.1. Chemicals and reagents

Generic chemicals were purchased from Sigma-Aldrich (St. Louis, USA), while reagents for 2D-DIGE were purchased from GE Healthcare (Uppsala, Sweden). The synthesis of the ICy3 and ICy5 dyes has been previously reported in our previous publication.[11] All primary antibodies were purchased from Genetex (Hsinchu, Taiwan), and anti-mouse and anti-rabbit secondary antibodies were purchased from GE Healthcare (Uppsala, Sweden). All of the chemicals and biochemicals used in this study were of analytical grade.

2.2. Cell lines and cell culture

The rat cardiomyocyte cell line H9C2 was purchased from the American Type Culture Collection (ATCC) (Manassas, VA) and was maintained in Dulbecco's modified Eagle's medium (DMEM) supplemented with 10% (v/v) FCS, L-glutamine (2 mM), streptomycin (100 μg mL^{-1}) and penicillin (100 IU mL^{-1}) (all from Gibco-Invitrogen Corp., UK). All cells were incubated in a humidified incubator at 37 °C and 5% CO_2. Cells were passaged at 80–90% confluence by trypsinization according to standard procedures.

2.3. Assay for endogenous reactive oxygen species using DCFH-DA

H9C2 cells (10 000 cells per well) were incubated with the indicated concentrations of doxorubicin for 20 min. After two washes with PBS, cells were treated with 10 μM of 2,7-dichlorofluorescin diacetate (DCFH-DA; Molecular Probes) at 37 °C for 20 min, and subsequently washed with PBS. Fluorescence was recorded at an excitation wavelength of 485 nm and an emission wavelength of 530 nm.

2.4. MTT cell viability assay

H9C2 cells growing exponentially were trypsinized, counted using a haemocytometer and 10 000 cells per well were seeded into 96-well plates. The culture was then incubated for 24 h before pre-treatment with the indicated concentrations of doxorubicin for 20 min or left untreated. After removal of the medium, 50 μL of MTT working solution (1 mg mL^{-1}) (Sigma) was added to the cells in each well, followed by a further incubation at 37 °C for 4 h. The supernatant was carefully removed. 100 μL of DMSO was added to each well and the plates shaken for 20 min. The absorbance of samples was then measured at 540 nm in a multi-well plate reader. Values were normalized against the untreated samples and were averaged from 4 independent measurements.

2.5. Flow cytometry analysis for apoptosis detection

An Annexin-V/propidium iodide (PI) double assay was performed using the Annexin V, Alexa Fluor® 488 Conjugate Detection kit (Life technologies). Following doxorubicin treatment, cells were typsinized from the culture dish and washed twice with cold PBS. 1×10^6 cells were resuspended in 500 μL binding buffer and stained with 5 μL Alexa Fluor® 488 conjugated Annexin V according to the manufacturer's instructions. 1 μL 100 μg mL^{-1} propidium iodide (PI) was added and mixed gently to incubate with cells for 15 min at room temperature in the dark. After the incubation period, samples were subjected to FCM analysis for 1 h using BD Accuri C6 Flow Cytometry (BD Biosciences, San Jose, CA). The data were analyzed using Accuri CFlow@ and CFlow Plus analysis software (BD Biosciences).

2.6. Redox-2D-DIGE and gel image analysis

For redox-DIGE analysis, cells were lysed in 2-DE buffer (4% w/v CHAPS, 8 M urea, 10 mM Tris-HCl pH 8.3 and 1 mM EDTA) in the presence of ICy3 or ICy5 (80 pmol mg^{-1} protein) on ice to limit post-lysis thiol modification. Test samples were labeled with the ICy5 dye and mixed with an equal amount of a standard pool of both samples labeled with ICy3. Since ICy dyes interfered with the protein assay, protein concentrations were determined on replica lysates not containing any dye. Lysates were left in the dark for 1 h followed by labeling with Cy2 to monitor protein levels. The reactions were quenched with DTT (65 mM final concentration) for 10 min followed by L-lysine (20-fold molar ratio excess of free L-lysine to Cy2 dye) for a further 10 min. Volumes were adjusted to 450 μL with buffer plus DTT and IPG buffer for rehydration. Isoelectric focusing was then performed using a Multiphor II apparatus (GE Healthcare) for a total of 62.5 kV h at 20 °C. Strips were then equilibrated in 6 M urea, 30% (v/v) glycerol, 1% SDS (w/v), 100 mM Tris-HCl (pH 8.8) with 65 mM dithiothreitol for 15 min, and then in the same buffer containing 240 mM iodoacetamide for a further 15 min. Equilibrated IPG strips were transferred onto 24 × 20 cm 12.5% polyacrylamide gels cast between low-fluorescence glass plates and bonded to one of the plates. The strips were overlaid with 0.5% (w/v) low melting point agarose in running buffer containing bromophenol blue. The gels were run in an Ettan Twelve gel tank (GE Healthcare) at 4 W per gel at 10 °C until the dye front had completely run off the bottom of the gels. Gels were then scanned directly between the glass plates using an Ettan DIGE Imager (GE Healthcare) according to the manufacturer's instructions. Image analysis was performed using DeCyder 2-D Differential Analysis Software v7.0 (GE Healthcare) to co-detect, normalize and quantify the protein features in the images. Features detected from non-protein sources were filtered out. All of the individual samples were run triplicate in this experiment and all of the statistic comparisons used in this assay were performed with two group paired Student *t*-test. Spots displaying a ≥ 1.3 average-fold increase or decrease in abundance with a P value < 0.05 were selected for protein identification.

2.7. Protein staining, in-gel digestion and MALDI-TOF/TOF MS analysis

Colloidal coomassie blue G-250 staining was used to visualize Cy-dye-labeled protein features in 2-DE followed by excised interested post-stained gel pieces for MALDI-TOF MS identification. The detailed procedures for protein staining, in-gel digestion, MALDI-TOF MS analysis and the algorithm used for data processing were described in our previous publication.[12] The spectrometer was also calibrated with a peptide calibration standard (Bruker Daltonics) and internal calibration

was performed using trypsin autolysis peaks at *m/z* 842.51 and *m/z* 2211.10. Peaks in the mass range of *m/z* 800–3000 were used to generate a peptide mass fingerprint that was searched against the Swiss-Prot/TrEMBL database (2010_04) with 515 203 entries using Mascot software v2.3.00 (Matrix Science, London, UK). The following parameters were used: *Rattus*; tryptic digest with a maximum of 1 missed cleavage; carbamidomethylation of cysteine, partial protein N-terminal acetylation, partial methionine oxidation, partial modification of glutamine to pyroglutamate, ICy3 (C_{34} H_{44} N_3 O) and ICy5 (C_{34} H_{42} N_3 O) and a mass tolerance of 50 ppm. Identifications were accepted based on significant MASCOT scores ($P < 0.05$), at least 4 peptides per protein, spectral annotation and observed *versus* expected molecular weight and p*I* on 2-DE. MALDI-TOF/TOF analysis was performed on the same instrument using the LIFT mode. MS/MS ion searches were performed using MASCOT with the same search parameters as above and using an MS/MS tolerance of ±0.2 Da.

2.8. Validation of thiol reactivity changes by immunoprecipitation coupled to immunoblotting

Doxorubicin-treated H9C2 cells were lysed in the presence of ICy3 or ICy5 dyes to limit post-lysis thiol modification. The labeling reactions were performed in the dark at 37 °C for 1 h and then quenched with a 2-fold molar excess of DTT for 10 min. 500 μg of ICy dye-labeled cell lysate was then diluted 20-fold with NP40 buffer containing protease inhibitors and then incubated with 5 μg of primary antibody and 40 μL of a 50% slurry of protein A-Sepharose for 16 h at 4 °C. Immune complexes were then washed three times in lysis buffer and boiled in Laemmli sample buffer prior to resolving by SDS-PAGE. ICy images were scanned directly between low-fluorescence glass plates using an Ettan DIGE Imager (GE Healthcare) followed by immunoblotting analysis with the same primary antibody to detect the specific protein. The immunoblotting procedure is described above.

2.9. Immunofluorescence

For immunofluorescence staining, cells were plated onto coverslips (VWR international) for overnight incubation. The cells were fixed with PBS containing 4% (v/v) paraformaldehyde for 25 min, washed three times with PBS, and followed by permeabilization in PBS containing 0.2% (v/v) Triton X-100 for 10 min. Coverslips were rinsed and blocked in PBS containing 5% (w/v) BSA for 10 min before incubation with primary antibodies diluted in 2.5% BSA/PBS for 1 h. After being washed three times with PBS, samples were incubated with the appropriate fluorescently labeled secondary antibodies diluted in 2.5% BSA/PBS for 1 h. Coverslips were then washed three times with PBS and at least twice with ddH_2O before mounting in Vectashield mounting medium (Vector Lab). Coverslip edges were sealed with nail polish onto glass slides (BDH) and then dried in the dark at 4 °C. For image analysis, cells were imaged using a Zeiss Axiovert 200 M fluorescent microscope (Carl Zeiss Inc., Germany). The laser intensities used to detect the same immunostained markers were identical, and none of the laser intensities used to capture images were saturated. Images were exported as .tif files using the Zeiss Axioversion 4.0.

3. Results

3.1. Doxorubicin induces generation of intracellular ROS in H9C2 cells

Previous reports have shown that doxorubicin is able to induce apoptosis in cardiomyocytes through the generation of ROS.[13,14] However, there is no report demonstrating the alteration of thiol reactivity on cysteine residues, since the free thiol group of cysteine residues is a potent nucleophilic agent, and is able to undergo a number of redox-induced modifications under physiological conditions. Using DCF fluorescence as the readout, the treatment of H9C2 cells with indicated concentrations of doxorubicin (0–40 μM) for 20 min resulted in a dose-dependent increase in ROS generation compared with untreated H9C2 cells (Fig. 1).

In order to evaluate the effect of short-term exposure of doxorubicin on H9C2 viability, we exposed H9C2 cells to the same dose range (0–40 μM) of doxorubicin for 20 min and performed MTT and apoptotic assays. The results showed no significant changes in cell viability and cell apoptosis during doxorubicin treatments (Fig. 1A and B) implying short-term treatment of doxorubicin in the indicated concentrations is able to induce ROS generation in cardiomyocytes, but not obviously interfere with H9C2 cell viability.

3.2. Redox proteomic analysis of doxorubicin-induced cysteine modifications of H9C2 proteins

Doxorubicin has been reported to induce cytotoxicity *via* ROS generation (see Introduction) and we also confirmed ROS

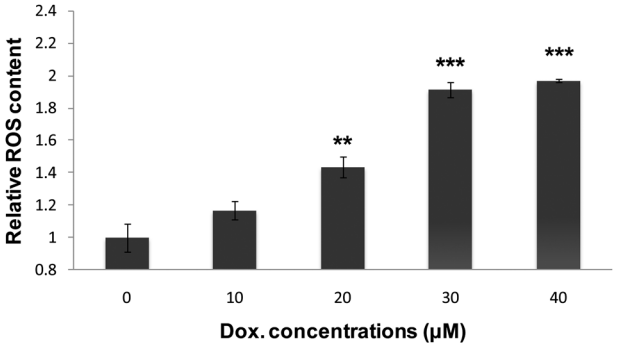

Fig. 1 MTT assay and flow cytometry analysis to monitor cell viability and cell apoptosis in response to indicated concentrations of doxorubicin. (A) MTT-based viability assays were performed on H9C2 cell cultures following treatments with different concentrations of doxorubicin (10 μM, 20 μM, 30 μM and 40 μM) or left untreated. Values were normalized against untreated samples and were the average of 4 independent measurements +/− the standard deviation. The statistical analysis was performed with two group paired Student *t*-tests. (B) H9C2 cells treated with different concentrations of doxorubicin were incubated with Alexa Fluor® 488 and propidium iodide in 1× binding buffer at room temperature for 15 min, and then stained cells were analyzed by flow cytometry to examine the effect of different doxorubicin concentrations on the apoptosis of H9C2 cells. Annexin V is presented in the *x*-axis as FL1-H, and propidium iodide is presented in the *y*-axis as FL2-H. The LR quadrant indicates the percentage of early apoptotic cells (Annexin V positive cells), and the UR quadrant indicates the percentage of late apoptotic cells (Annexin V positive and propidium iodide positive cells).

generation in cardiomyocytes (Fig. 2). We thus hypothesized that doxorubicin-induced ROS might deregulate or damage cellular proteins by oxidative modification of their cysteinyl thiol groups. Hence, we applied a recently developed redox-2D-DIGE strategy utilizing iodoacetylated ICy dyes[15] to assess doxorubicin-induced changes in cardiac protein thiol reactivity. Doxorubicin-treated (40 μM/20 μM) or vehicle-treated H9C2 cells were lysed in the presence of ICy5 in triplicate. Individual ICy5-labeled samples were then run on 2D gels against an equal load of a ICy3-labeled standard pool comprised of an equal mixture of both sample types to aid in spot matching and to improve the accuracy of quantification (Fig. 3). The ICy5-labeled samples were subsequently labeled with lysine Cy2 dye as an internal protein level control, which was used to normalize the corresponding ICy5/ICy3 signals. In total 1854 protein features were detected, of which 82 displayed statistically significant differences in labeling due to doxorubicin treatment (Fig. 3). CCB post-staining and matching with fluorescence images allowed confident picking of 62 gel features, and 25 of these were identified as unique gene products by MALDI-TOF peptide mass fingerprinting or MALDI-TOF/TOF peptide sequence analysis (Table 1 and Fig. 3). For example, the redox-2D-DIGE combining peptide sequencing profiles listed in Fig. 4C contribute to the identification of nucleoside diphosphate kinase A (NDK A), which shows a 1.60-fold and 1.71-fold increase of ICy signals treated with 20 μM and 40 μM doxorubicin in comparison with no treatment, respectively (Fig. 5C). Subsequent validation of the alterations of thiol reactivity of the identified proteins by combined immunoprecipitation with immunoblotting showed that the free thiol group levels were increased 1.21-fold and 1.34-fold during 20 μM and 40 μM doxorubicin treatment in comparison with no treatment (Fig. 5C). The results further confirm the accuracy of redox-2D-DIGE on monitoring the changes of free thiol content of cardiac proteins. Also, the same experimental design confirmed that the free thiol content of beta-tubulin and calumenin changed during doxorubicin treatment (Fig. 5A and B). Notably, the differentially labeled proteins were mostly cytoplasmic and fell into several functional groups, including protein folding, translation regulation, biosynthesis, intracellular transport, calcium binding, glycolysis, mitotic control and protein degradation (Fig. 6).

3.3 Doxorubicin-induced changes in cell morphology and cytoskeleton organization

Our redox-proteomic analysis revealed the involvement of doxorubicin-induced cardiotoxicity in dysregulation of protein

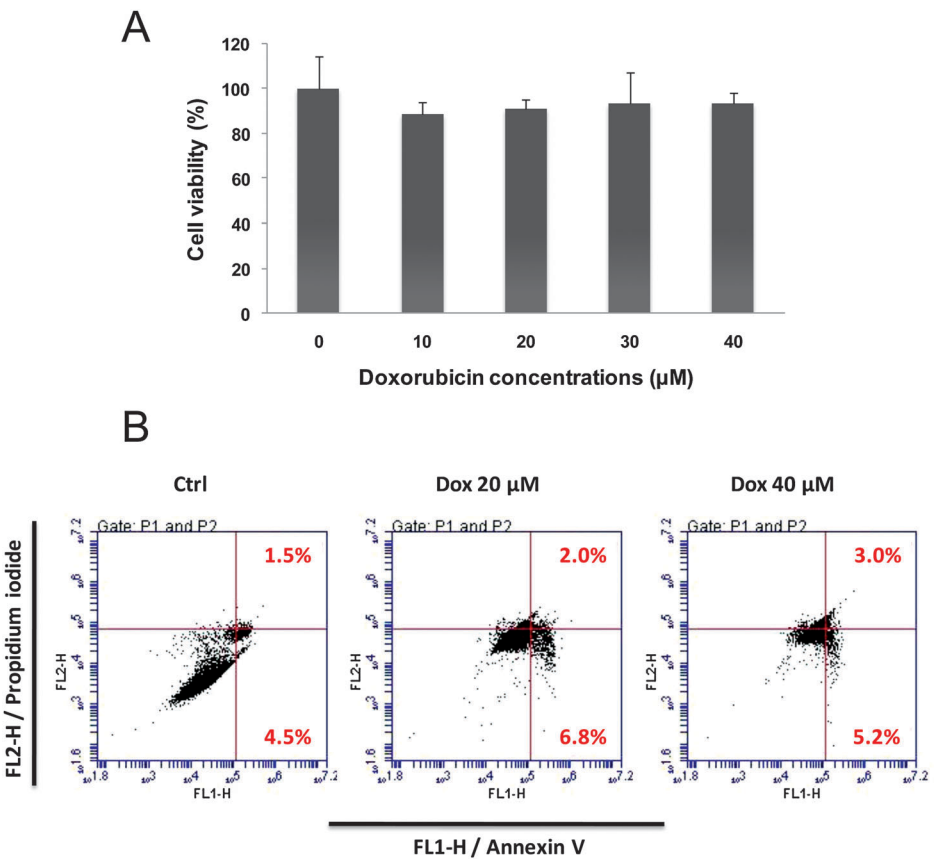

Fig. 2 DCFH assay to monitor doxorubicin-induced intracellular ROS in H9C2 cells. DCFH-based intracellular ROS production assays were performed where 100 000 H9C2 cells were plated into 24-well plates in medium containing 10% FBS. After 24 h, the cells were treated with the indicated concentrations of doxorubicin for a further 20 min. Cells were then treated with 10 μM of DCFH-DA at 37 °C for 20 min and the fluorescence was recorded at excitation and emission wavelengths of 485 nm and 530 nm, respectively. Values were normalized against untreated samples and were the average of 4 independent measurements +/− the standard deviation. All of statistical comparisons used in this assay were performed with two group paired Student *t*-tests.

folding, translational regulation and cytoskeleton regulation. The high proportion of proteins identified with roles in cytoskeletal regulation and cytoskeleton organization prompted us to examine the effect of doxorubicin treatment on the cytoskeletal proteins (F-actin and beta-tubulin) expression, localization and organization. The immunofluorescence results indicated that doxorubicin treatment resulted in modification of the actin cytoskeleton and tubulin with a loss of cytoplasmic filamentous tubulin, a loss of cytoplasmic stress fibers of actin and the loss of uniform cell shape with the altered distributions of actin and tubulin in H9C2 cells (Fig. 7). Notably, the DAPI nucleus stains were significantly reduced in doxorubicin treated H9C2 cells implying that a possible fluorescence quench might take place between doxorubicin and the DAPI dye due to the emission wavelength of DAPI overlapping with the excitation wavelength of doxorubicin (480 nm).

4. Discussion

Myocardial damage induced by doxorubicin is mainly due to the generation of ROS. If one can understand the molecular targets of doxorubicin-induced ROS, then the doxorubicin-induced myocardial dysfunction could be prevented or alleviated. Based on this concept, several studies have evaluated the effects of doxorubicin and the protective mechanism on myocardial ischemia in animals and patients.[16,17] However, an incomplete understanding of the roles of ROS on doxorubicin-induced myocardial ischemia, together with the seemingly conflicting results regarding the effects of antioxidants have discouraged their therapeutic application. In this study, we examined the molecular mechanisms of doxorubicin-induced cytotoxicity in cardiomyocytes *in vitro.* Using 2D-DIGE and MALDI-TOF/TOF MS, 25 unique doxorubicin-modulated alterations in protein thiol reactivity have been identified in H9C2 cells. The results demonstrate that this strategy is powerful enough to identify a broad-ranging signature in response to doxorubicin-induced cardiac injury, with the altered protein thiol reactivity having main roles in protein folding, translational regulation and cytoskeleton regulation. Although the overall coverage of protein mixtures identified by LC-based mass spectrometry analysis is generally recognized to be higher than that of 2-DE-based protein analysis, 2-DE-based proteomic analysis offers the benefit of direct protein quantification at the protein level with reduced analytical variation.[7] Our study also demonstrated that treatment of H9C2 cells with doxorubicin results in the generation of ROS. Since ROS can activate multiple signaling pathways, regulate a variety of cellular activities and modulate disease progression, it is essential to study the molecular events related to their effects. In addition, ROS are reported to modify protein cysteinyl thiol groups, leading to oxidative damage.[18–20] Hence, our previously established cysteine-labeling 2D-DIGE strategy using ICy3/ICy5 dyes was used to determine the altered protein thiol reactivity in H9C2 due to ROS generation.

The ICy labeling data presented supports the hypothesis that doxorubicin can induce the formation of free thiols in certain proteins through disruption of disulphide bonds; meanwhile, doxorubicin-induced ROS might directly oxidize thiol groups to form the sulfenic, sulfinic or sulfonic acid forms of cysteine, which would not interact with the ICy dyes. These thiol modifications have been reported to perturb the normal functions of the proteins.[21] In the current study, twenty-five proteins with differential thiol reactivity were identified by MALDI-TOF and/or MALDI-TOF/TOF MS. Identified proteins, such as nucleoside diphosphate kinase A and phosphoglycerate kinase 1 are reported to maintain cell metabolism, and both displayed an increase in ICy dye labeling following doxorubicin treatment (Table 1). Thus, their cysteine residues must be reduced to generate new thiol groups for ICy labeling, implying possible oxidative damage and deregulation of these proteins. Phosphoglycerate kinase 1 was found to be altered significantly by doxorubicin treatment, suggestive of direct oxidative modification. In support of this observation, we found reduced ICy labeling of phosphoglycerate kinase 1 after treatment with doxorubicin. The modulation of the phosphoglycerate kinase 1 supports that oxidative stress can redirect carbohydrate fluxes into the pentose phosphate pathway to generate increased reducing power in the form of NADPH at the expense of glycolysis.

In contrast, several of the identified cytoskeleton proteins, such as vimentin and cofilin-1, displayed a decrease in ICy dye

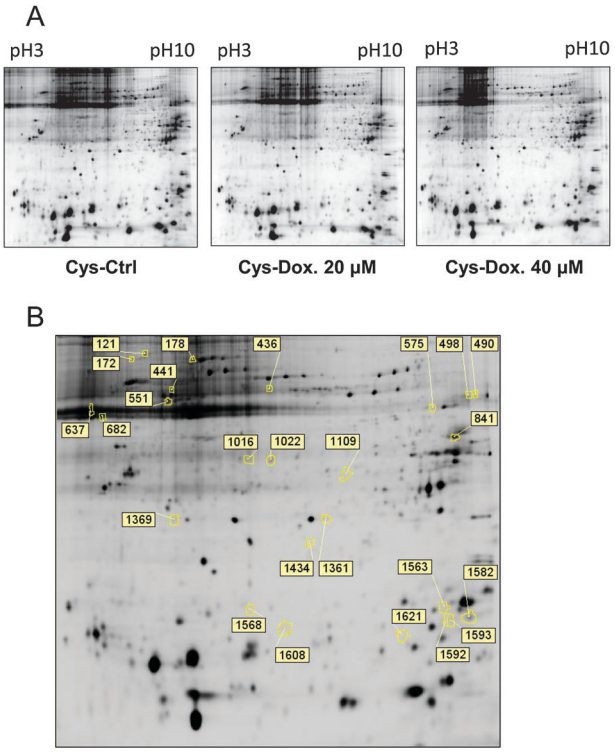

Fig. 3 Analysis of doxorubicin-induced cysteine-modification in H9C2 cells with cysteine labeling 2D-DIGE. (A) Lysates from H9C2 cells treated with 20 μM/40 μM of doxorubicin or left untreated were subjected to redox 2D-DIGE analysis as described in the Materials and Methods section. Images of protein samples from untreated and doxorubicin-treated H9C2 are displayed. (B) Differentially labeled protein features are annotated with spot numbers.

Table 1 Differential cysteine labeled proteins identified by ICy 2D-DIGE and MALDI-TOF/TOF MS. Proteins displaying doxorubicin-induced differential labeling of cysteines and lysines using ICy dyes and NHS-Cy2 dyes, respectively, were identified by MALDI-TOF peptide mass mapping and MS/MS sequence analysis. Proteins displaying an average fold-difference of ≥1.3-fold where $p < 0.05$ and spots matched in all images are in italic

Spot no.	Swiss-prot no.	Protein name	p*I*	MW	No. match. peptides	Coverage (%)	Score	Subcellular location	Function	Matched peptides[b]	Dox 20 μM/Ctrl[c]	Dox 40 μM/Ctrl[c]	Dox 40 μM/ Dox 20 μM[c]
121	P06761	78 kDa glucose-regulated protein/Grp78	5.07	72 473	10/16	16	95/51	Endoplasmic reticulum	Protein folding	IINEPTAAAIAYGLDKR FEELNMDLFR	*−1.70*	*−1.64*	1.04
121	P06761	78 kDa glucose-regulated protein/Grp78[a]	5.07	72 473	1/1	2	126/51	Endoplasmic reticulum	Protein folding	DNHLLGTFDLTGIPPAPR VTHAVVTVPAYFNDAQR	*−1.70*	*−1.64*	1.04
172	P06761	78 kDa glucose-regulated protein/Grp78[a]	5.07	72 473	1/1	1	67/51	Endoplasmic reticulum	Protein folding	ITPSYVAFTPEGER DNHLLGTFDLTGIPPAPR	*1.54*	*2.22*	*1.44*
1582	P15178	Aspartyl-tRNA synthetase, cytoplasmic	6.02	57 546	5/19	14	57/51	Cytoplasm	Translation regulation	DLTVQKADEVVWVR ETLINKGFVEIQTPK	*−1.30*	−1.19	1.10
637	O35783	Calumenin[a]	4.40	37 087	1/1	2	58/51	Endoplasmic reticulum	Ca-binding protein	EQFVEFR	*−1.35*	1.10	*1.50*
637	O35783	Calumenin[a]	4.40	37 087	1/1	5	63/51	Endoplasmic reticulum	Ca-binding protein	DWILPSDYDHAEAEAR	*−1.35*	1.10	*1.50*
1563	P45592	Cofilin-1[a]	8.22	18 749	1/1	1	75/51	Nucleus matrix	Cytoskeleton regulation	YALYDATYETK	*−1.54*	−1.20	1.28
1563	P45592	Cofilin-1[a]	8.22	18 749	1/1	1	101/51	Nucleus matrix	Cytoskeleton regulation	HELQANCYEEVKDR	*−1.54*	−1.20	1.28
551	Q6AYH5	Dynactin subunit 2	5.14	44 235	5/14	15	73/51	Cytoplasm	Intracellular transport	YADLPGIAR VHQLYETIQR	*1.34*	*1.50*	1.12
178	P63018	Heat shock cognate 71 kDa protein/HspA8	5.37	71 055	7/26	13	74/51	Cytoplasm	Protein folding	TVTNAVVTVPAYFNDSQR TTPSYVAFTDTER	1.07	*−1.53*	*−1.64*
178	P63018	Heat shock cognate 71 kDa protein/HspA8[a]	5.37	71 055	1/1	2	112/51	Cytoplasm	Protein folding	TVTNAVVTVPAYFNDSQR TTPSYVAFTDTER	1.07	*−1.53*	*−1.64*
1369	P42930	Heat shock protein beta-1/Hsp27[a]	6.12	22 936	1/1	4	64/51	Cytoplasm	Protein folding	LFDQAFGVPR	1.16	*1.33*	1.14
1434	P42930	Heat shock protein beta-1/Hsp27[a]	6.12	22 936	1/1	1	80/51	Cytoplasm	Protein folding	LFDQAFGVPR	*1.54*	1.07	*−1.44*
841	Q6URK4	Heterogeneous nuclear ribonucleoprotein A3	9.10	39 856	5/12	21	60/51	Nucleus	Translation regulation	LFIGGLSFETTDDSLR GFAFVTFDDHDTVDK	1.28	−1.02	*−1.30*
841	Q6URK4	Heterogeneous nuclear ribonucleoprotein A3[a]	9.10	39 856	1/1	1	60/51	Nucleus	Translation regulation	LFIGGLSFETTDDSLR	1.28	−1.02	*−1.30*
436	Q8VHV7	Heterogeneous nuclear ribonucleoprotein H	5.70	49 442	4/14	14	59/51	Nucleus	Translation regulation	GLPWSCSADEVQR HTGPNSPDTANDGFVR	*1.34*	1.18	−1.12
1608	Q05982	Nucleoside diphosphate kinase A/NDK A[a]	5.96	17 296	1/1	1	108/51	Cytoplasm	Biosynthesis	TFIAIKPDGVQR DRPFFSGLVK	*1.60*	*1.71*	1.07
1621	P19804	Nucleoside diphosphate kinase B	6.92	17 386	2/2	13	193/51	Cytoplasm	Biosynthesis	TFIAIKPDGVQR GDFCIQVGR	1.26	−1.19	*−1.50*
1592	P10111	Peptidyl-prolyl *cis-trans* isomerase A[a]	8.34	18 091	1/1	10	118/51	Cytoplasm	Protein folding	VNPTVFFDITADGEPLGR	*−1.48*	*−2.79*	*−1.88*
1593	P10112	Peptidyl-prolyl *cis-trans* isomerase A[a]	8.34	18 091	1/1	8	78/51	Cytoplasm	Protein folding	IIPGFMCQGGDFTR	−1.08	*1.37*	*1.47*
1593	P10112	Peptidyl-prolyl *cis-trans* isomerase A[a]	8.34	18 091	1/1	10	161/51	Cytoplasm	Protein folding	VNPTVFFDITADGEPLGR	−1.08	*1.37*	*1.47*
575	P16617	Phosphoglycerate kinase 1[a]	8.02	44 909	1/1	1	84/51	Cytoplasm	Glycolysis	LGDVYVNDAFGTAHR	*1.34*	1.20	−1.10
575	P16617	Phosphoglycerate kinase 1[a]	8.02	44 909	1/1	4	59/51	Cytoplasm	Glycolysis	ALESPERPFLAILGGAK	*1.34*	1.20	−1.10
1109	P18420	Proteasome subunit alpha type-1[a]	6.15	29 784	1/1	1	60/51	Cytoplasm	Protein degradation	FVFDRPLPVSR	*−1.37*	*−1.35*	1.01
1361	Q9JIR1	RIMS-binding protein 2	5.06	116 283	7/16	9	57/51	Plasma membrane	Intracellular transport	VQSEQFNLLSR YQFFNLRPNMAYK	*−1.61*	−1.09	*1.46*
682	Q9WVC0	Septin-7	8.82	50 818	10/26	18	66/51	Cytoplasm	Mitosis regulation	THMQDLK MEMEMEQVFEMK	1.29	*1.34*	1.04

Table 1 (*continued*)

Spot no.	Swiss-prot no.	Protein name	p*I*	MW	No. match. peptides	Coverage (%)	Score	Subcellular location	Function	Matched peptides[b]	Dox 20 μM/Ctrl[c]	Dox 40 μM/Ctrl[c]	Dox 40 μM/Dox 20 μM[c]
490	P29457	Serpin H1	8.88	46 602	4/10	13	61/51	Endoplasmic reticulum	Protein folding	DNQSGSLLFIGR LYGPSSVSFADDFVR	*1.39*	*−2.33*	*−3.22*
498	P29457	Serpin H1[a]	8.88	46 602	1/1	1	133/51	Endoplasmic reticulum	Protein folding	LYGPSSVSFADDFVR	*1.45*	*−1.41*	*−2.05*
1568	P13668	Stathmin[a]	5.76	17 278	1/1	1	116/51	Cytoplasm	Cytoskeleton regulation	ASGQAFELILSPR	*1.61*	*−1.07*	*−1.72*
1022	Q6P9T8	Tubulin beta-2C chain	4.79	50 225	4/9	9	57/51	Cytoplasm	Cytoskeleton	FPGQLNADLR YLTVAAVFR	*−1.07*	*−1.37*	*−1.27*
1016	P69897	Tubulin beta-5 chain[a]	4.78	50 095	1/1	1	67/51	Cytoplasm	Cytoskeleton	FPGQLNADLR	*−1.89*	*−1.03*	*1.82*
441	P31000	Vimentin[a]	5.06	53 757	1/1	1	100/51	Nucleus	Cytoskeleton	SLYSSSPGGAYVTR ISLPLPNFSSLNLR	*−1.84*	*−1.56*	1.17

[a] Proteins identified by MALDI-TOF/TOF. [b] In MS analysis, we listed 2 representative peptide sequences in the matched peptide column. In MS/MS analysis, we listed the MS/MS-sequenced peptide in the matched peptide column. [c] To accurately calculate doxorubicin-induced differential labeling of cysteines in consideration of protein level alterations, the cysteine-labeling ratios were normalized using the lysine-labeling ratios.

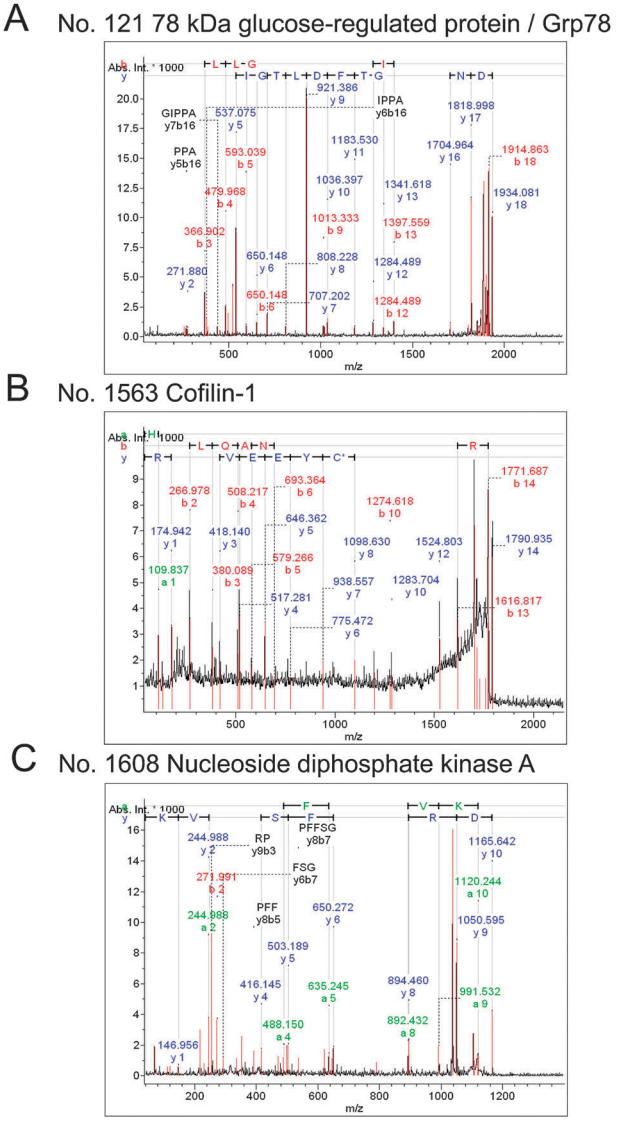

Fig. 4 Protein identification by MALDI-TOF/TOF sequence analysis. (A) 78 kDa glucose-regulated protein/Grp78, (B) Cofilin-1 and (C) nucleoside diphosphate kinase A were resolved by MALDI-TOF/TOF MS.

labeling following doxorubicin treatment (Table 1). As a result, their free thiol groups must be oxidized in response to doxorubicin treatment to block ICy labeling, implying possible oxidative damage and deregulation of these proteins. Cofilin-1 is an actin depolymerizing factor (ADF) that is responsible for the disassembly of actin filament. It controls actin filament dynamics and is essential for cell proliferation, migration and cell cycle progression.[22] Our immunostain study also confirmed the inference that doxorubicin treatment resulted in the loss of cytoplasmic stress fibers of actin and the loss of a uniform cell shape with the altered distributions of actin in H9C2 cells. The deregulation of cofilin is associated with various cancers, such as colon cancer and breast cancer.[23,24] In addition, cofilin-1 activity is also modulated by oxidation. Klamt *et al.* found that oxidation of cofilin induces the loss of actin-binding ability and stimulated the release of cytochrome c,

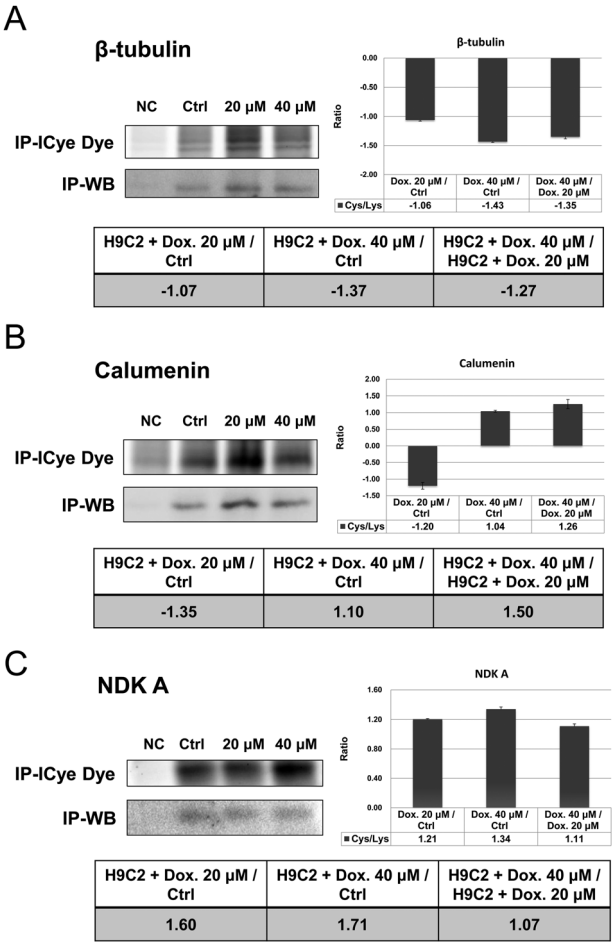

Fig. 5 Immunoprecipitation combining immunoblotting to validate identified proteins (beta-tubulin, calumenin and nucleoside diphosphate kinase A) with cysteine modifications in doxorubicin-treated H9C2 cells. ICy dye-labeled protein samples from H9C2 cells were either untreated or treated with 20 μM/40 μM of doxorubicin followed by immunoprecipitatied with Grp78, cofilin-1 and nucleoside diphosphate kinase A antibody to confirm the alterations of thiol reactivity in Grp78, cofilin-1 and nucleoside diphosphate kinase A, respectively. The image was visualized by an Ettan DIGE imager (top-left panels). Immunoblotting against the corresponding antibody was performed to gain the protein level (top-left panels). The normalized ratios between ICy dye signal and protein immunoblotted level are shown in the top-right panels. The standardized abundances between ICy dye signal and NHS-Cy2 signal from DeCyder software are shown in the bottom panels. All of results were calculated from three independent IP-WB experiments.

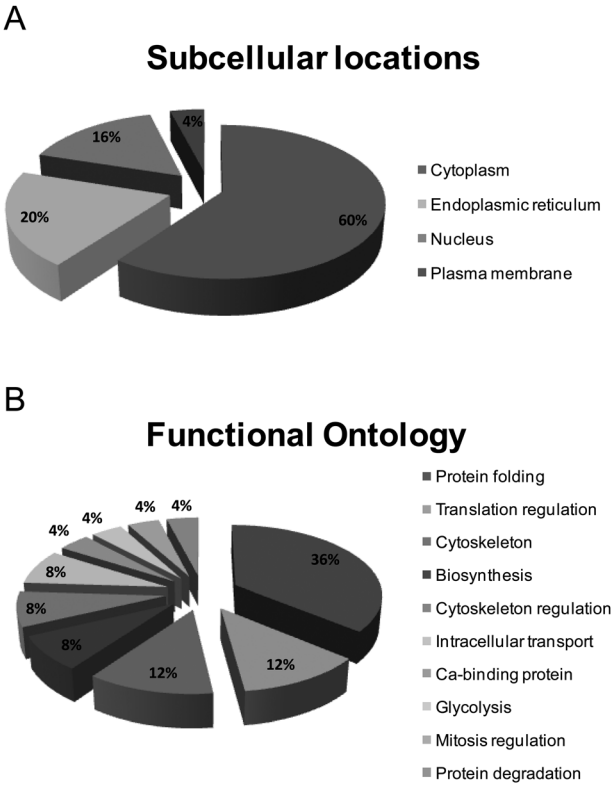

Fig. 6 Distribution of differential ICy-labeled proteins from doxorubicin-treated and untreated H9C2 cells according to (A) subcellular location and (B) biological function.

and induced cell apoptosis.[25] In our redox proteomic analysis, we observed that cofilin-1 decreases labeling in normalized cysteine levels on doxorubicin-treated H9C2 cells implying cofilin-1 is in an oxidative status after doxorubicin treatment, which might affect the actin filament dynamics, induce cell apoptosis and reduce the process of wound healing.

Although cysteine labeling 2D-DIGE can be used to monitor thiol reactivity alteration of target proteins, there are some limitations of the technique used in this study. Firstly, the cysteine-labeling 2D-DIGE experiment is based on fluorescence-based protein thiol group quantification, which can detect a sub-nanogram level of ICy dye-labeled proteins; in contrast, our post-staining experiment is based on modified CCB staining with a sensitivity of around 20–50 nanograms.[11] Accordingly, numerous differential ICy dye-labeled low-abundant proteins can be detected by a fluorescent scanner, but failed to be visualized with CCB staining. This is the reason why just more than 50% of the differential labeling features on cysteine labeling 2D-DIGE can be picked for MALDI-TOF and/or MALDI-TOF/TOF MS identification. Secondly, the cysteine labeling 2D-DIGE technique can only be used to monitor the free thiol group modifications on cysteine residues; however, this technique can not tell what kinds of cysteine modifications (sulfenic, sulfinic, sulfonic or glutathionated modifications) take place. Last but not least, the cysteine labeling strategy uses a high dye to protein ratio (80 pmol dye/μg protein) for redox-2D-DIGE analysis to increase the sensitivity of the detection of thiol-containing proteins. However, the high dye to protein level increases protein precipitation and decreases the total resolved protein spots.

In conclusion, the present study offers an insight into the mechanisms of doxorubicin-induced apoptosis in cardiomyocytes and shows a link between ROS generation and the cell damaging process. The findings of this study may have clinical implications in that doxorubicin treatment has been routinely used in destroying fast-growing cancer cells, but with the serious side-effect of cardiotoxicity. Additionally, numerous identified cellular targets might be useful for the evaluation of heart damage induced by doxorubicin.

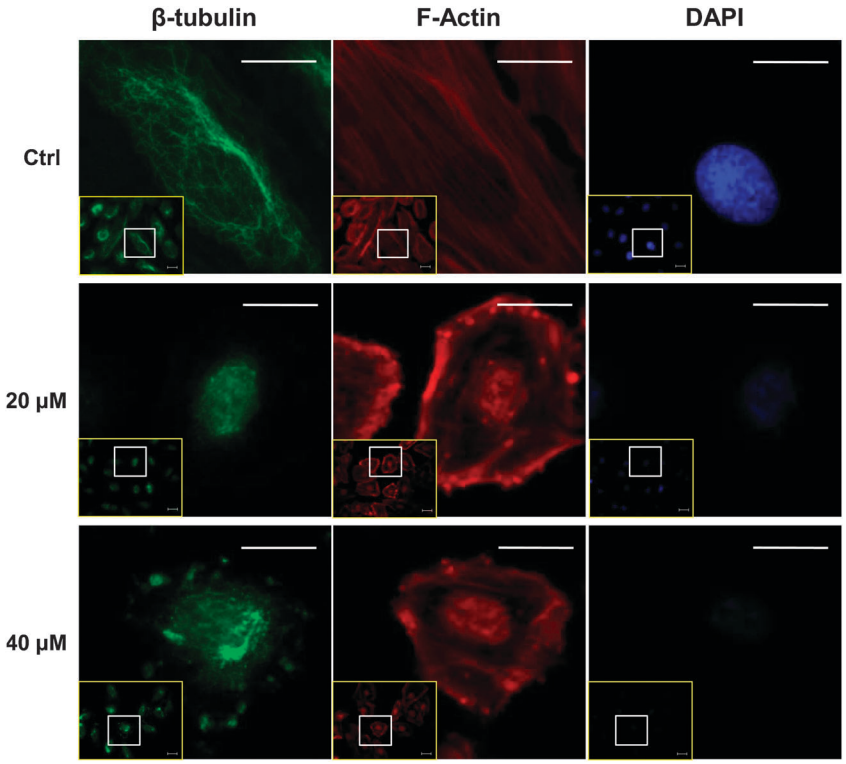

Fig. 7 Immunofluorescence analysis of morphological and protein organization changes in H9C2 cells in response to doxorubicin treatment. 5×10^4 H9C2 cells were seeded on cover slips for 24 h. The cells were treated with the indicated concentrations of doxorubicin for a further 20 min before fixation and staining for beta-tubulin, F-actin and DAPI. Each set of three fields was taken using the same exposure, and images are representative of three different fields. Scale bar = 20 μm.

Abbreviations

2-DE	Two-dimensional gel electrophoresis
CCB	Colloidal coomassie blue
CHAPS	3-[(3-Cholamidopropyl)-dimethylammonio]-1-propanesulfonate
ddH_2O	Double deionized water
DIGE	Differential gel electrophoresis
DTT	Dithiothreitol
FCS	Fetal calf serum
MALDI-TOF MS	Matrix assisted laser desorption ionization-time of flight mass spectrometry
TFA	Trifluoroacetic acid

Conflict of interest statement

The authors declare that there are no conflicts of interest.

Acknowledgements

This work was supported by a NSC grant (100-2311-B-007-005 and 101-2311-B-007-011) from National Science Council, Taiwan, NTHU and CGH grant (100N2723E1) from National Tsing Hua University, NTHU Booster grant (99N2908E1) from National Tsing Hua University, Toward World-Class University project from National Tsing Hua University (100N2051E1).

References

1 S. Verma, S. Dent, B. J. Chow, D. Rayson and T. Safra, *Cancer Treat. Rev.*, 2008, **34**, 391–406.
2 R. Vatsyayan, P. Chaudhary, P. C. Lelsani, P. Singhal, Y. C. Awasthi, S. Awasthi and S. S. Singhal, *Int. J. Oncol.*, 2009, **34**, 1505–1511.
3 A. E. Green and P. G. Rose, *Nanomedicine*, 2006, **1**, 229–239.
4 S. Christiansen and R. Autschbach, *Eur. J. Cardio-Thorac. Surg.*, 2006, **30**, 611–616.
5 E. V. Kalishina, A. N. Saprin, V. S. Solomka, N. P. Shchebrak and L. A. Piruzian, *Vopr. Onkol.*, 2003, **49**, 294–298.
6 T. Simunek, M. Sterba, O. Popelova, M. Adamcova, R. Hrdina and V. Gersl, *Pharmacol. Rep.*, 2009, **61**, 154–171.
7 J. F. Timms and R. Cramer, *Proteomics*, 2008, **8**, 4886–4897.
8 H. C. Chou, Y. C. Lu, C. S. Cheng, Y. W. Chen, P. C. Lyu, C. W. Lin, J. F. Timms and H. L. Chan, *J. Proteomics*, 2012, **75**, 3158–3176.
9 C. L. Wu, H. C. Chou, C. S. Cheng, J. M. Li, S. T. Lin, Y. W. Chen and H. L. Chan, *J. Proteomics*, 2012, **75**, 1991–2014.
10 H. L. Chan, J. Sinclair and J. F. Timms, *Methods Mol. Biol.*, 2012, **854**, 113–128.
11 H. L. Chan, S. Gharbi, P. R. Gaffney, R. Cramer, M. D. Waterfield and J. F. Timms, *Proteomics*, 2005, **5**, 2908–2926.
12 T. C. Lai, H. C. Chou, Y. W. Chen, T. R. Lee, H. T. Chan, H. H. Shen, W. T. Lee, S. T. Lin, Y. C. Lu, C. L. Wu and H. L. Chan, *J. Proteome Res.*, 2010, **9**, 1302–1322.
13 D. L. Keefe, *Semin. Oncol.*, 2001, **28**, 2–7.

14 P. K. Singal, T. Li, D. Kumar, I. Danelisen and N. Iliskovic, *Mol. Cell. Biochem.*, 2000, **207**, 77–86.
15 H. L. Chan, P. R. Gaffney, M. D. Waterfield, H. Anderle, M. H. Peter, H. P. Schwarz, P. L. Turecek and J. F. Timms, *FEBS Lett.*, 2006, **580**, 3229–3236.
16 M. Mokni, S. Hamlaoui-Guesmi, M. Amri, L. Marzouki, F. Limam and E. Aouani, *Cardiovasc. Toxicol.*, 2012, **12**, 158–165.
17 J. M. Calvo-Romero, R. Fernandez-Soria-Pantoja, J. D. Arrebola-Garcia and M. Gil-Cubero, *Ann. Pharmacother.*, 2001, **35**, 1403–1405.
18 M. Kemp, Y. M. Go and D. P. Jones, *Free Radical Biol. Med.*, 2008, **44**, 921–937.
19 J. V. Cross and D. J. Templeton, *Antioxid. Redox Signaling*, 2006, **8**, 1819–1827.
20 L. K. Moran, J. M. Gutteridge and G. J. Quinlan, *Curr. Med. Chem.*, 2001, **8**, 763–772.
21 P. Ghezzi, V. Bonetto and M. Fratelli, *Antioxid. Redox Signaling*, 2005, **7**, 964–972.
22 C. H. Tsai, S. J. Chiu, C. C. Liu, T. J. Sheu, C. H. Hsieh, P. C. Keng and Y. J. Lee, *Cell Cycle*, 2009, **8**, 2365–2374.
23 D. Nowak, A. J. Mazur, A. Popow-Wozniak, A. Radwanska, H. G. Mannherz and M. Malicka-Blaszkiewicz, *Eur. J. Histochem.*, 2010, **54**, e14.
24 Y. Zhang and X. Tong, *J. Int. Med. Res.*, 2010, **38**, 1042–1048.
25 F. Klamt, S. Zdanov, R. L. Levine, A. Pariser, Y. Zhang, B. Zhang, L. R. Yu, T. D. Veenstra and E. Shacter, *Nat. Cell Biol.*, 2009, **11**, 1241–1246.

